Anharmonicity, solvation forces, and resolution in atomic force microscopy at the solid-liquid interface

Kislon Voïtchovsky[*,†]

Institute of Materials, School of Engineering, École Polytechnique Fédérale de Lausanne (EPFL), 1015 Lausanne, Switzerland

(Received 14 May 2013; revised manuscript received 9 July 2013; published 28 August 2013)

Solid-liquid interfaces are central to nanoscale science and technology and control processes as diverse as self-assembly, heterogeneous catalysis, wetting, electrochemistry, or protein function. Experimentally, measuring the structure and dynamics of solid-liquid interfaces with molecular resolution remains a challenge. This task can, in principle, be achieved with atomic force microscopy (AFM), which functions locally, and with nanometer precision. When operated dynamically and at small amplitudes, AFM can provide molecular-level images of the liquid solvation layers at the interfaces. At larger amplitudes, results in the field of multifrequency AFM have shown that anharmonicities in the tip motion can provide quantitative information about the solid's mechanical properties. The two approaches probe opposite aspects of the interface and are generally seen as distinct. Here it is shown that, for amplitudes $A < d$, the thickness of the solvation region, the tip mainly probes the interfacial liquid, and subnanometer resolution can be achieved through solvation forces. For $A > d$, the tip trajectory becomes rapidly anharmonic due to the tip tapping the solid, and the resolution decreases. A nonlinear transition between the two regimes occurs for $A \sim d$ and can be quantified with the second harmonic of the tip oscillation. These results, confirmed by computer simulations, remain valid in most experimental conditions. Significantly, they provide an objective criterion to enhance resolution and to decide whether the results are dominated by the properties of the solid or of the liquid.

DOI: 10.1103/PhysRevE.88.022407 PACS number(s): 68.37.Ps, 31.70.Dk, 68.08.−p

I. INTRODUCTION

Solid-liquid interfaces are at the center of countless phenomena, ranging from charge and heat transfer [1] to electrochemistry [2], the folding and function biomolecules [3], heterogeneous catalysis [4], self-assembly processes [5], and controlled wetting [6]. All these processes are controlled by the particular organization of the liquid molecules close to the surface of the solid [7]. Experimentally, measuring the structure and dynamics of solid-liquid interfaces locally and with nanometer resolution remains a challenge, and most available data stem either from diffraction experiments averaging over large areas of the interface [8] or from theory [9] and simulation [10].

Recent advances in the field of atomic force microscopy (AFM) have demonstrated that, when operated dynamically and fully immersed in liquid, AFM can derive quantitative information about the local structure [11,12] and free solvation energy [13] of the interfacial liquid, often with molecular- or atomic-level resolution. This type of measurement is typically achieved by oscillating an AFM probe with subnanometer amplitudes at the interface so as to explore the solvation layers formed by the liquid close to the surface of the solid [11–14]. When operated in this regime [small-amplitude AFM (SA-AFM)], the trajectory of the vibrating tip is generally assumed purely harmonic.

In parallel, developments in the field of multifrequency AFM (MF-AFM) [15–20] have established that, in liquid, the nonlinear tip-sample interaction can induce momentary excitation of higher harmonics during the tip oscillation cycle. This momentary excitation is related to the solid's viscoelastic properties and can be exploited to gain compositional contrast over soft samples [17,18]. Multifrequency studies generally use larger tip oscillation amplitudes (typically $A > 10$ nm) [16,17,20] so as to ensure appropriate detection of higher harmonics. The lateral resolution reported for this regime is typically an order of magnitude lower than for experiments carried out with subnanometer amplitudes.

The two approaches, developed separately, probe opposite aspects of the interface: SA-AFM mainly senses the interfacial liquid, whereas, MF-AFM probes the properties of the solid. Yet experimentally, these approaches can only be differentiated by the amplitude with which the probe is oscillated [21] with SA-AFM measurements carried out at small amplitudes (typically, $A \lesssim 1$ to 2 nm) and MF-AFM measurements carried out at larger amplitudes (typically, $A \gtrsim 10$ nm). This suggests that, for a given cantilever at the solid-liquid interface, the part of the interface probed (solid or liquid) can be tuned simply by adjusting the regime of amplitude at which the cantilever is oscillated. In this picture, SA-AFM and MF-AFM correspond to regimes located each at one extremity of the amplitude range available to AFM operators in liquid.

To date, the transition between both regimes is still largely unexplored. Understanding the behavior of the transition region is of fundamental importance for dynamic AFM measurements in liquid, first, to provide a correct interpretation for AFM results. The vast majority of published studies relying on dynamic AFM in liquid operate in a regime that corresponds to a medium ground between SA-AFM and MF-AFM. Second, any quantitative interpretation of the data requires a model of the tip dynamics. Since both regimes rely on very different interactions between the tip, the interfacial liquid and the solid, no single model is currently applicable at all operating amplitudes, and different theories are required to describe

[*]kislon.voitchovsky@epfl.ch

[†]Address from 1 October 2013: Department of Physics, University of Durham, Durham DH1 3HP, United Kingdom, kislon.voitchovsky@durham.ac.uk

SA-AFM [14,22,23] and MF-AFM [16,17] results. Finally, an appropriate choice of amplitude may simultaneously provide information about both the solid and the liquid at the interface while retaining molecular- or atomic-level resolution, further emphasizing the need to correctly understand the transition region.

Here, the full transition between both regimes has been studied experimentally and with computer simulations [24] for solids exhibiting different stiffnesses and affinities for the interfacing liquid, water. As the free oscillation of the vibrating lever is progressively increased, all systems show a nonlinear transition from a harmonic oscillation regime dominated by solvation forces in the interfacial liquid to an anharmonic regime where the mechanical properties of the sample become increasingly important. The vibration amplitude at which the transition occurs is determined by the solvation characteristics of the interface with little or no influence from the solid's mechanical properties. Significantly, best imaging conditions were consistently achieved in the harmonic regime, and a progressive loss of resolution could be directly correlated with the apparition of anharmonicities in the tip trajectory.

II. ATOMIC FORCE MICROSCOPY

The experiments were conducted in amplitude modulations (AMs) with a commercial AFM and both the sample and the cantilever fully immersed in water. The stiffness of the selected cantilever (nominal stiffness $k_c = 0.76$N/m) is similar to that used in typical AFM experiments on soft samples in liquid. In AM-AFM, the cantilever is driven near its resonance frequency ν_{res}. The free vibration amplitude A_0 of the cantilever is set while the cantilever is several microns away from the sample. As the base of the vibrating cantilever approaches the sample, the tip vibration amplitude A progressively decreases until a chosen adjustable value A_{set}. The surface is then scanned keeping A_{set} constant with a feedback loop while the phase lag φ between the driving and the tip oscillations is allowed to vary freely. Topographic images of the sample are obtained from the corrections imposed by the feedback loop. The relative set point is defined as

$$S = A_{\text{set}}/A_0, \tag{1}$$

with both A_{set} and A_0 taken at ν_{res}. S provides an indication of the imaging conditions. High S values (typically, $S > 0.8$) correspond to soft imaging conditions, whereas, lower values (typically $S < 0.7$) impose harsher conditions. As the tip oscillates at the solid-liquid interface, contributions from both the sample and the interfacial liquid can influence the tip trajectory, depending on the experimental conditions, namely, A_0 and S. Practically, controlling S can become difficult at large amplitudes due to contributions from higher harmonics in the tip motion. Throughout this study, the value of S provided was, therefore, backcalculated from experimentally measured tip trajectories (see the Supplemental Material [25] for details) after adjusting the imaging conditions as close as possible to the desired 'medium' ($S \sim 0.75$), 'soft' ($S \sim 0.85$), or 'ultra-soft' ($S \sim 0.95$) conditions. Using this approach, the provided S value accurately quantifies the imaging conditions, even if the latter are subjectively determined.

In order to disentangle contributions from the solid and the liquid, solids with different Young moduli E have been investigated, always in water. All the solids are hydrophilic but exhibit different works of adhesions W with water. Three solids were selected: calcite, mica, and stacks of mixed 1,2-dipalmitoyl-*sn*-glycero-3-phosphocholine/1,2-dipalmitoyl-*sn*-glycero-3-phospho-(1′-rac-glycerol) (sodium salt) (DPPC/DPPG) lipid bilayers. Their typical characteristics are $E_{\text{calcite}} = 80$G Pa [26] and $W_{\text{calcite}} = 92 \pm 7$ mN/m [13], $E_{\text{mica}} = 80$G Pa [27] and $W_{\text{mica}} = 140 \pm 10$ mN/m [13], and $E_{\text{bilayer}} = 20$ MPa [28] and $W_{\text{bilayer}} = 95 \pm 10$ mN/m [29], respectively. The idea is to use calcite as a reference system; mica presents a comparable stiffness but a higher affinity for water, whereas, the lipid stacks present a lower stiffness but a comparable affinity for water.

A typical set of experiments is presented in Fig. 1 for calcite. The surface was imaged with free amplitudes A_0 ranging from ~ 0.4 to more than 12 nm, and for each A_0, three different set points corresponding to ultrasoft, soft, and medium scanning conditions were tested. Representative images are shown in Figs. 1(a)–1(e) for selected A_0 together with the corresponding tip trajectory obtained directly from the AFM photodiode during the image acquisition using a separate oscilloscope. Best imaging conditions are typically achieved with ultrasoft to soft set points [13,30,31].

Comparing the images sequences in Figs. 1(a)–1(e) reveals a loss in resolution as A_0 increases beyond 1.14 nm with the images becoming progressively noisier. The loss in resolution correlates with the apparition of anharmonicity in the tip trajectory as higher harmonics of ν_{res} are momentarily stimulated when the tip contacts the sample. Interestingly, for $A_0 \gtrsim 5$ nm, experimentally reducing the imaging set point (i.e., decreasing the distance between the sample and the base of the cantilever) almost exclusively increases the anharmonicity with no significant decreases in the measured S value [see Fig. 1(g)]. For all the imaging conditions, the total anharmonicity H in the tip motion is defined as

$$H = \sum_{i>1} \frac{A\,(\nu = i\,\nu_{\text{res}})}{A_{\text{set}}}. \tag{2}$$

H increases nonlinearly with A_0; this is particularly visible for ultrasoft imaging conditions in Fig. 1(e). Two main H regimes can be identified: for $A_0 \lesssim 1$ nm, H increases slowly with A_0, and a clear influence of S over H is visible. In this regime, $H < 15\%$. For $A_0 \gtrsim 5$ nm, H remains almost constant with $H \gtrsim 30\%$ regardless of S. A rapid transition between these two regimes occurs continuously between ~1 and 5 nm. This transition is almost exclusively due to the apparition of a second harmonic in the tip trajectory; higher harmonics appear at larger A_0 with no obvious order of apparition (see Fig. 2 in the Supplemental Material [25]). Highest resolution images are consistently achieved in the first imaging regime where H is lower. In order to better quantify this transition and to provide an objective transition amplitude $A_{0,t}$, the experimental data were fitted with the Hill equation,

$$H = \frac{H_{\max}}{1 + \left[\frac{A_{0,t}}{A_0}\right]^{\xi}}, \tag{3}$$

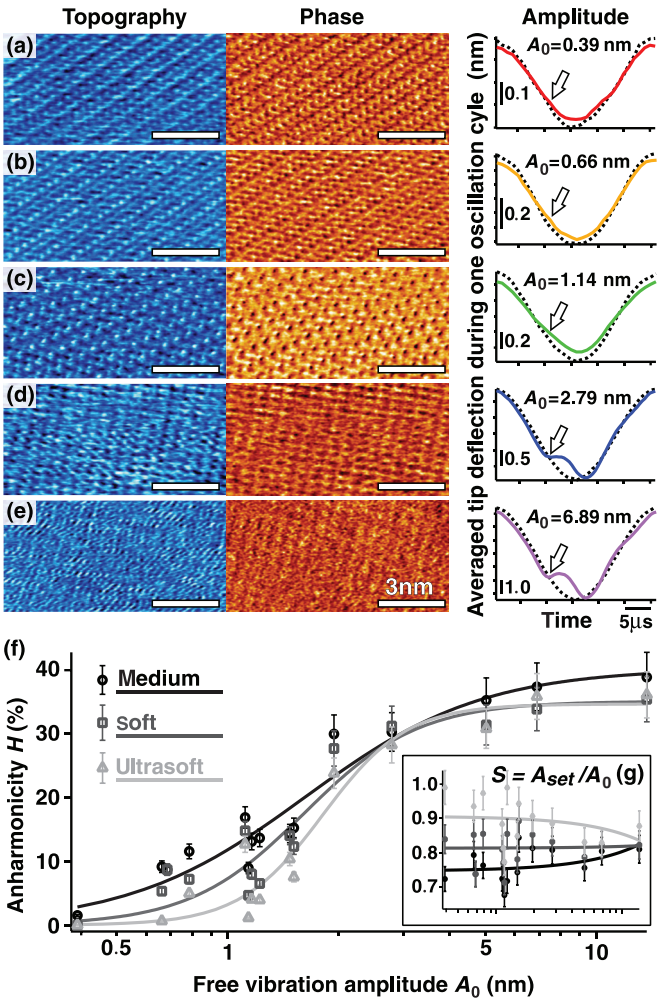

FIG. 1. (Color online) AM-AFM imaging of the surface of calcite in water as a function of A_0 and S. Images acquired in soft conditions ($S \sim 0.8$) are presented in (a)–(e) for selected A_0 values. In each case, a full cycle of the tip trajectory recorded during the image acquisition is given (solid curve) together with the free trajectory, recorded away from the surface in identical operating conditions (dotted black curve). The curves presented have been averaged over >1000 cycles (always preserving the phase), but the motion of the base of the cantilever has not been subtracted. Significant anharmonicities arise when the tip reaches the surface for $A_0 > 1.14$ nm (arrows). The total anharmonicity H is given in (f) for each imaging condition over all the A_0 studied. The fits of the experimental data were obtained with the Hill equation which provided transition amplitude values of $A_{0,t} = 1.8 \pm 0.3$ nm (medium), $A_{0,t} = 1.6 \pm 0.2$ nm (soft), and $A_{0,t} = 1.8 \pm 0.2$ nm (ultrasoft). The H values were obtained by summing the intensities of the harmonics peaks in the fast Fourier transform spectra of the tip trajectory (see the Supplemental Material [25] for an example of the analysis). An abrupt increase in H is visible for $A_0 \gtrsim 1.5$ nm regardless of the imaging condition used, although lower S tend to yield higher H. (g) The inset provides the S values measured experimentally for each A_0 and each imaging condition. The curves are linear fits of the experimental data. The differences between imaging conditions are less marked for larger A_0. This is due to the large anharmonicities making it difficult to fully control the amplitude at the fundamental frequency. The color scale of the topography (blue) is always 5 Å in (a)–(e), and the color scale of the phase (yellow) is adjusted in each case to provide the best contrast.

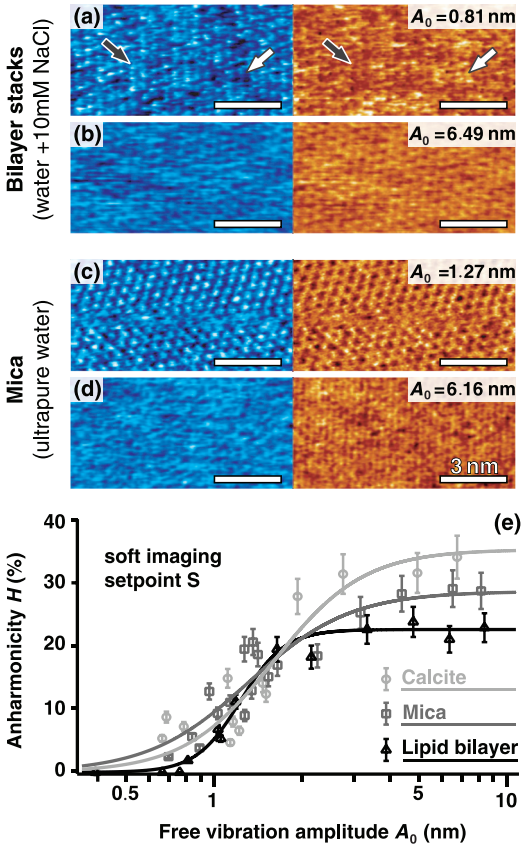

FIG. 2. (Color online) AM-AFM imaging of the surface of bilayers stacks (a) and (b) and mica (c) and (d) in water as a function of A_0. All images were acquired with a soft set point. As for Fig. 1, the topography is presented on the left (blue color scale), and the phase is presented on the right (yellow color scale). (a) When imaged with small amplitude (that is, below the H transition), the tip probes the interfacial liquid and can distinguish between molecular solvation structures. These differences are interpreted as molecular-level signatures of the type of lipid images: The more strongly hydrated PG headgroups (black arrow) appear higher in topography and darker in phase than the PC (white arrow). The phase contrast reflects the magnitude of the local solvation forces [13]. Different structural arrangements of the PC and PG headgroups might also play a role (see the Supplemental Material [25] for further discussions) (b) At higher amplitudes (above the H transition), the lipid headgroups can still be resolved but without a clear distinction between DPPG and DPPC. Similar results on mica show atomic-level imaging of the solvation structure at small amplitude (c) and complete loss of resolution with apparition of noise at larger amplitudes (d). (e) Evolution of H as a function of A_0 for all three solids in soft imaging conditions. (The data for medium and ultrasoft set points is available for both systems in the Supplemental Material [25] together with control experiments for the lipids). The color scales for the images (a)–(d) are as in Fig. 1.

where H_{max} is the maximum anharmonicity reached in the considered imaging conditions and ξ is an empirical exponent related to the abruptness of the transition. Interestingly, the fits always yielded the same $A_{0,t}$ value within uncertainty ($A_{0,t} = 1.7 \pm 0.3$nm) regardless of the imaging set point. The latter only influenced the abruptness of the transition with

smoother transitions for smaller S values. The existence of a unique transition amplitude for all imaging conditions was also verified in computer simulations (presented hereafter) and suggests the transition to reflect a physical characteristic of the interface.

In order to identify the origin of the transition, the same experiment was carried out on mica and on the lipid bilayer stacks. The results are summarized with selected images in Fig. 2. All samples induced a nonlinear increase in anharmonicity with A_0 with a transition $A_{0,t}$ between 1.5 and 2 nm regardless of the sample stiffness.

The experiments on the lipids allow for a direct interpretation of these two anharmonicity regimes. Variations in the local hydration structure of the bilayer due to the two types of lipids present can clearly be distinguished for $A_0 < A_{0,t}$ [Fig. 2(a)], whereas, only the hexagonal packing of the lipids is visible at larger A_0. Since the only difference between the two lipids is the dissimilar affinity of their respective headgroup for water (their hydrophobic part is identical), the contrast between the two types of lipids unambiguously demonstrates that the AFM images local variations in the hydration structure at the surface are induced by the different headgroups and not the surface itself. At higher amplitudes ($A_0 > A_{0,t}$), contributions from the solid start to dominate, and the chemical contrast, only present in the interfacial liquid, is lost [Fig. 2(b)].

Factors other than the chemical composition of the lipids are likely to induce nanoscale variations within the interfacial liquid, but the overall argument remains valid with such variations only visible at small imaging amplitudes.

The anharmonicity is more marked for the stiffer samples at large amplitudes. The transition is also less abrupt for mica, which has the highest affinity for water. These considerations together with the existence of a similar H transition for all samples suggest the transition to be governed by the interfacial liquid. This is also consistent with the near absence of anharmonicity in air for comparable experiments [32].

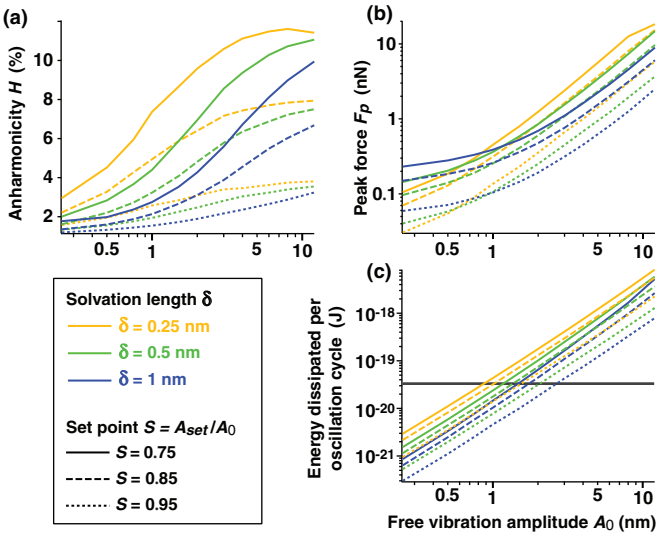

FIG. 3. (Color online) (a) Simulation of the oscillation anharmonicity H, (b) the maximum force experienced by the tip during an oscillation cycle (peak force), and (c) the tip energy dissipation per oscillation cycle as a function of A_0 for several set point values and solvation decay lengths. In (a), the transition amplitudes $A_{0,t}$ were obtained from fits with the Hill equation: For $\delta = 0.25$ nm [light gray curves (orange)], $A_{0,t}^{S=0.75} = 0.7 \pm 0.1$, $A_{0,t}^{S=0.85} = 0.7 \pm 0.1$, and $A_{0,t}^{S=0.95} = 0.6 \pm 0.1$ nm ($S = 0.95$); for $\delta = 0.5$ nm [gray curves (green)], $A_{0,t}^{S=0.75} = 1.6 \pm 0.2$, $A_{0,t}^{S=0.85} = 1.7 \pm 0.2$, and $A_{0,t}^{S=0.95} = 2.1 \pm 0.9$ nm ($S = 0.95$); for $\delta = 1.0$ nm [black curves (blue)], $A_{0,t}^{S=0.75} = 8 \pm 5$, $A_{0,t}^{S=0.85}$, and $A_{0,t}^{S=0.95}$ nm did not converge properly. The dark horizontal line in (c) marks the energy necessary to fully remove water from 0.5×0.5 nm^2 of calcite.

III. COMPUTER SIMULATIONS

The actual meaning of $A_{0,t}$ cannot, however, be directly deduced from the AFM results. In order to overcome this difficulty, computer simulations of the system were carried out using the virtual environment for dynamic AFM ([VEDA] [24]). In VEDA, the variables experimentally measured in standard dynamic AFM measurements are directly simulated as a function of the operating parameters. Although the simulation is based on continuum mechanics and fluid dynamics, it can provide direct insight into the physical parameters influencing the tip motion, a task, at present, impossible with molecular dynamics or atomistic simulation approaches. Significantly, the simulation takes into account solvation forces, which are assumed to decay exponentially away from the solid (see the Supplemental Material [25] for details on the simulation parameters). Solvation forces are generally more complex and can show some oscillatory behavior with alternate attractive and repulsive regions [11,33]. Their modeling with an exponential decay is, hence, not strictly correct, but it captures the fact well that their magnitude decreases rapidly, typically, over a few molecular diameters [8,11,34] when moving away from the surface of the solid. Furthermore, the experimental conditions used in the present study (in particular, the relatively low cantilever stiffness), did not reproducibly capture oscillatory solvation forces but rather a short-range monotonic dissipation increase close to the surface [13]. A precise mapping of the solvation forces could, in principle, be obtained with stiffer cantilevers and smaller oscillations amplitudes [11], but such a task is beyond the scope of this paper. Results simulating typical experimental conditions on calcite for several set points and decay lengths δ of the solvation forces are presented in Fig. 3.

Given the nature of the simulation, it is not possible to make a fully quantitative comparison with experimental data. Nonetheless, the simulation results show a remarkable agreement with the experimental trends with a rapid nonlinear increase in H with A_0 [Fig. 3(a)]. The transition between the two H regimes is not as marked as in the experimental curves, but $A_{0,t}$ values can, nonetheless, be obtained when fitting the H curves with the Hill equation (Fig. 3 caption). The resulting $A_{0,t}$ values show a direct dependence on δ (namely, $A_{0,t} \propto e^{-1/\delta}$), clearly indicating that the transition is governed by solvation forces at the interface: for $A_0 < A_{0,t}$, the tip oscillates within the interfacial liquid, and its trajectory is mostly harmonic. As A_0 reaches $A_{0,t}$, the tip begins to tap directly on the solid. This abrupt transition from a highly dissipative liquid environment to a stiff elastic solid momentarily stimulates higher harmonics upon impact of the tip on the

surface. This can be directly observed in the peak interaction forces F_p experienced by the oscillating tip [Fig. 3(b)]. F_p is always repulsive and increases with A_0 following two regimes with a transition around $A_{0,t}$. For $A_0 < A_{0,t}$, F_p is dominated by solvation forces; it increases weakly with A_0, and the strongest repulsion is felt for the system with the longest range of solvation forces. As for H, smaller S also increase F_p. The trend is reversed for $A_0 > A_{0,t}$ since the tip transverses more easily, the interface exhibiting the shortest δ;F_p is now dominated by tapping on the solid and increases significantly more rapidly with A_0, regardless of the set point value.

IV. GENERAL DISCUSSION

Taken together, the experimental and simulation results have several important consequences. First, it is possible to choose whether to study the structure and properties of the solid or of the liquid at the interface simply by adjusting A_0 so as to select the desired regime. At the transition, the tip should provide sufficient energy to fully probe the solvation layers of the liquid without significantly stimulating higher harmonics. Experimentally, this condition can be met by selecting a cantilever with sufficient stiffness as illustrated in Fig. 3(c) for a simulated water-calcite interface. In the first approximation, the condition can be expressed in amplitude modulation as

$$\frac{1}{2Q}k\delta^2 \sim W_{sl}\alpha, \tag{4}$$

with k as the stiffness of the lever, Q as its quality factor in liquid, δ as the thickness of the interfacial liquid region ($A_{0,t} \sim \delta$), W_{sl} as the solid-liquid work of adhesion, and α as the area of interface being fully probed by the tip. Typically, $\alpha \sim \varepsilon^2$, where ε is the resolution achieved (here, $\alpha \sim 0.5 \times 0.5$ nm^2). Interestingly, the results presented here suggest that, under typical working conditions for soft samples in liquid, most AFM studies mainly probe the interfacial liquid at the surface of the considered sample rather than the sample itself. However, for many soft samples, such as living cells or polymer brushes, the effective stiffness of the interfacial liquid as described phenomenologically by Eq. (4) might be larger than that of the sample, hence, making it impossible for the AFM tip to travel through the solvation layers without significantly deforming the sample.

Second, since anharmonicities appear detrimental to resolution, their minimization should improve the imaging resolution [35]. This can, indeed, be verified for lipid bilayers where the abrupt change in repulsive force experienced by the tip as it reaches the solid is less marked than for the stiffer minerals: Molecular resolution could still be achieved with large A_0 on the soft lipids stacks despite the loss of solvation-dominated imaging [see Fig. 2(b)]. Consistently, the H values are also smaller for the lipids. This last consideration suggests that anharmonicities could be used as a quantifiable means to ensure optimum imaging conditions, especially since higher harmonics first appear through the second harmonic.

Finally, close to the transition, it should be possible to work in a regime allowing for the probing of both the solid and the liquid properties simultaneously while maintaining high resolution. Such a regime, demonstrated here for lipid stacks, is, however, likely to depend on the system investigated and, in particular, on a limited difference in stiffness between the interfacial liquid and the solid.

V. CONCLUSIONS

In conclusion, the results presented here show that, when investigating solid-liquid interfaces with dynamic AFM, both the liquid and the solid can be probed distinctively depending on the vibration amplitude of the tip. The anharmonicity in the tip trajectory is an important indicator of the medium probed with a rapid increase in anharmonicity as the tip contacts the solid.

ACKNOWLEDGMENTS

This work was conducted following a suggestion from R. Garcia who is gratefully acknowledged. The author would also like to thank A. Raman for insightful conversations regarding the computer simulations and F. Stellacci for making the AFM available. Funding from the Swiss National Science Foundation (Ambizione Award) is gratefully acknowledged.

[1] T. Ohara and D. Suzuki, Microscale Thermophys. Eng. **4**, 189 (2000).
[2] M. Hugelmann, P. Hugelmann, W. Lorenz, and W. Schindler, Surf. Sci. **597**, 156 (2005).
[3] H. Frauenfelder, P. Fenimore, G. Chen, and B. McMahon, Proc. Natl. Acad. Sci. USA **103**, 15469 (2006).
[4] J.-M. Andanson and A. Baiker, Chem. Soc. Rev. **39**, 4571 (2010).
[5] G. Whitesides and P. Laibinis, Langmuir **6**, 87 (1990).
[6] L. Gao and T. McCarthy, Langmuir **25**, 14105 (2009).
[7] K. Wandelt and S. Thurgate, *Solid-Liquid Interfaces: Macroscopic Phenomena, Microscopic Understanding* (Springer, Berlin, 2003).
[8] P. Fenter and N. Sturchio, Prog. Surf. Sci. **77**, 171 (2004).
[9] D. Chandler, Nature (London) **437**, 640 (2005).
[10] N. Giovambattista, P. Debenedetti, and P. Rossky, J. Phys. Chem. C **111**, 1323 (2007).
[11] T. Fukuma, Y. Ueda, S. Yoshioka, and H. Asakawa, Phys. Rev. Lett. **104**, 016101 (2010).
[12] K. H. Sheikh and S. P. Jarvis, J. Am. Chem. Soc. **133**, 18296 (2011).
[13] K. Voïtchovsky, J. J. Kuna, S. A. Contera, E. Tosatti, and F. Stellacci, Nat. Nanotechnol. **5**, 401 (2010).
[14] S. de Beer, D. van den Ende, and F. Mugele, Nanotechnology **21**, 325703 (2010).
[15] R. Garcia and E. T. Herruzo, Nat. Nanotechnol. **7**, 217 (2012).
[16] X. Xu, J. Melcher, S. Basak, R. Reifenberger, and A. Raman, Phys. Rev. Lett. **102**, 060801 (2009).
[17] A. F. Payam, J. R. Ramos, and R. Garcia, ACS Nano **6**, 4663 (2012).
[18] A. Raman, S. Trigueros, A. Cartagena, A. P. Z. Stevenson, M. Susilo, E. Nauman, and S. A. Contera, Nat. Nanotechnol. **6**, 809 (2011).

[19] S. D. Solares, J. Appl. Phys. **111**, 054909 (2012).
[20] O. Sahin, S. Magonov, C. Su, C. F. Quate, and O. Solgaard, Nat. Nanotechnol. **2**, 507 (2007).
[21] Although subtleties may arise for the different feedback modes, the argument should generally remain valid.
[22] S. V. Patil and P. Hoffmann, Adv. Eng. Mater. **7**, 707 (2005).
[23] J. E. Sader and S. P. Jarvis, Phys. Rev. B **74**, 195424 (2006).
[24] J. Melcher, S. Hu, and A. Raman, Rev. Sci. Instrum. **79**, 061301 (2008).
[25] See Supplemental Material at http://link.aps.org/supplemental/10.1103/PhysRevE.88.022407 for a full description of the data analysis, control experiments, and additional discussions.
[26] J. Zhao, B. Zhou, B. Liu, and W. Guo, J. Comput. Theor. Nanosci. **6**, 1181 (2009).
[27] L. E. McNeil and M. Grimsditch, J. Phys.: Condens. Matter **5**, 1681 (1993).
[28] L. Picas, F. Rico, and S. Scheuring, Biophys. J. **102**, L01 (2012).
[29] The different W values given here were calculated from SA-AFM data using a procedure described elsewhere [13].
[30] M. Ricci, P. Spijker, F. Stellacci, J.-F. Molinari, and K. Voïtchovsky, Langmuir **29**, 2207 (2013).
[31] K. Voïtchovsky and M. Ricci, Proc. SPIE **8232**, 823200 (2012).
[32] R. Garcia, C. J. Gómez, N. F. Martinez, S. Patil, C. Dietz, and R. Magerle, Phys. Rev. Lett. **97**, 016103 (2006).
[33] T. Fukuma, M. J. Higgins, and S. P. Jarvis, Phys. Rev. Lett. **98**, 106101 (2007).
[34] J. Israelachvili, *Intermolecular and Surface Forces*, 2nd ed. (Academic, London, 1992).
[35] H. V. Guzman, A. P. Perrino, and R. Garcia, ACS Nano **7**, 3198 (2013).